IEEE Access
Multidisciplinary | Rapid Review | Open Access Journal

Received January 18, 2022, accepted February 5, 2022, date of publication February 14, 2022, date of current version March 1, 2022.

Digital Object Identifier 10.1109/ACCESS.2022.3151425

Transient Stability Enhancement of Grid Integrated Wind Energy Using Particle Swarm Optimization Based Multi-Band PSS4C

AHMAD ADEL ALSAKATI[1], (Graduate Student Member, IEEE), CHOCKALINGAM ARAVIND VAITHILINGAM[1], (Senior Member, IEEE), JAMAL ALNASSEIR[2], KANENDRA NAIDU[3], AND GOWTHAMRAJ RAJENDRAN[1], (Graduate Student Member, IEEE)

[1]High Impact Research Laboratory, Faculty of Innovation and Technology, Taylor's University Lakeside Campus, Subang Jaya, Selangor Darul Ehsan 47500, Malaysia
[2]Electric Power Engineering Department, Faculty of Mechanical an Electrical Engineering, Damascus University, Damascus, Syria
[3]School of Electrical Engineering, College of Engineering, Universiti Teknologi MARA (UiTM), Shah Alam, Selangor Darul Ehsan 40450, Malaysia

Corresponding author: Jamal Alnasseir (jamalnasseir@yahoo.de)

This work was supported by Taylor's University through its Taylor's Research Scholarship Programme under Grant TUFR/2017/001/01.

ABSTRACT There is a growing need for stability enhancement in modern electrical networks integrated with wind energy, particularly due to different oscillation modes disturbances. Power system stabilizers (PSSs) are used to mitigate oscillations and improve the stability of the power system. This paper presents a comprehensive analysis of single-band PSS1A and multi-band PSS4C (MB-PSS4C) connected to the ST1A excitation system. An efficient approach in the selection of the parameters of MB-PSS4C using Particle Swarm Optimization (PSO) is proposed. A comparative investigation linked to the common Pattern Search and Simplex Search, from previous work, has been conducted to gauge the efficacy of PSO. The generator's transient stability with considerations of relative power angle (power angle differences), speed deviation, and active power of synchronous generators (SGs) are analyzed. Different wind penetration levels ranging from 36MW to 108 MW are integrated into the network and are investigated. Results demonstrate that PSO-MB-PSS4C connected to ST1A stabilizes the system effectively with reduced settling time while mitigating the peak power angle differences of SGs. Reduced settling time of 1.35 s is observed for wind penetration of 48 MW, with 43.31° peak power angle; while for high wind penetration of 108 MW, the settling time is around 8 s with peak power angle of 43.9°.

INDEX TERMS Multi-band PSS4C, power system stabilizer, particle swarm optimization, transient stability, wind energy.

I. INTRODUCTION

In recent years, environmental aspects, fossil fuel depletion, and increased energy demands propelled the integration of renewable energy technologies into power systems [1], [2]. Wind energy is one of the fastest-growing and matured renewable energy sources across the world [2]–[4]. However, wind energy relies on wind speed, weather, and terrain. Due to the unpredictable nature of wind speed, wind turbines may not consistently generate the same amount of electricity as conventional sources. Therefore, the integration of wind energy makes challenges on power system stability [4]–[7] and creates adverse effects on system stability.

The associate editor coordinating the review of this manuscript and approving it for publication was Siqi Bu.

System stability is one of the most significant problems that should be addressed towards increased reliability. It can be categorized into different classifications, such as small-disturbance stability, transient stability, and voltage stability. In this research, transient stability is considered, which is the ability of a power system to remain synchronized after a severe disturbance [8], such as three-phase fault (considered as the most severe fault) [9], loss of transmission line, or significant increase of load [10]. Disturbances occur mainly in the form of oscillations, which include three main oscillation modes. The local mode refers to the swinging of one generator at the power station against the remains of the system. Inter-area mode is correlated with the generators' swinging in one area against generators in other areas [11]. The frequency of local-area mode ranges from 0.7 Hz to

2.0 Hz, and the frequency of inter-area oscillation is within the range of 0.1–0.8 Hz [12]. On the other hand, the global mode is related to the swinging of all machines when the frequency of oscillation is very low, ranging from 0.01 Hz to 0.05 Hz [13].

As the effects of these oscillations can be severe, it is required to mitigate the system's instability issues for power system operation and planning purposes. Various forms of controls may be applied to improve system stability by using devices such as FACTS [9], STATCOM [14], [15], and Static Var Compensator (SVC) [14]. However, a Power System Stabilizer (PSS) is considered as an effective solution for damping oscillations [13], [16], [17] as it improves the stability margin and network reliability.

Improved PSS can cope with different oscillation modes [7], [18]. This requirement led to the development of MB-PSS with multi-band transfer functions that offer higher levels of flexibility and reliability compared to Conventional PSS (CPSS) for the different oscillation modes [7], [18], [19]. MB-PSS4B is developed based on multiple frequency bands and consists of three bands that are correlated with different oscillation modes. Each band comprises gains, filters, and limiter [20]. Speed deviation and active power of Synchronous Generators (SGs) are used as inputs to MB-PSS [21], [22].

Additionally, PSS parameters must be defined accurately to achieve better response under severe disturbances. A failure in the comprehensive tuning approach may destabilize the power system. Studies have been carried out on the different optimization methods used to tune PSS. Three optimization algorithms (culture, PSO and co-evolutionary algorithms) were combined to propose a design for MB-PSS to select the PSS parameters [19]. The results of the proposed design showed suppressing the oscillations under loading conditions, compared to the other MB-PSS designs. In [13], the authors proposed an improved modal performance index as objective function minimization to tune PSS4B, which is effective in damping different oscillation modes compared to that of the conventional PSS1A.

Focusing on enhancing the transient stability of the power grid, Didier and Leveque (2016) [10] compared different types of PSS and optimized the placement of Superconducting Fault Current Limiter (SFCL). The authors demonstrated the effectiveness of the optimal resistive value of SFCL in mitigating the angular separation variation of SGs.

Considering system uncertainties, Bhukya and Mahajan (2019) [4] investigated how static series synchronous compensator and PSS can enhance the stability of wind energy that is incorporated into the IEEE standard network. The research examined small-signal and transient stability using the eigenvalue approach and time-domain simulation, where speed deviation served as the objective function for PSO. The study reported enhanced system stability, mitigated oscillations, and improved damping ratio. In [14], PSO was implemented to select the parameters of PSS, SVC, and STATCOM by taking into consideration the eigenvalue as the objective function. The linearization of a nonlinear system was performed to analyze system stability and mitigate oscillations effectively Huang *et al.* (2020) [23] applied the MB-PSS to an interconnection power system with the implementation of wind energy. The researchers summarized that improved frequency stability together with the local and inter-area modes damping using MB-PSS.

Static synchronous compensator with Multi-Band Power Oscillation Damper (MB-POD) was implemented to dampen the low-frequency oscillations in the multi-machine power system [15]. The MB- POD was used to control the voltage through the voltage modulation with tuning the controllers under different operating conditions using eigenvalue and damping ratio analysis.

An actual power system was considered with wind energy to analyze the dynamic responses of the system with the power system stabilization of the wind turbines [24]. The work showed a 180° phase shift between the oscillations of the speed of SG and the power of wind turbine causing a damping effect due to the phase shift. The active power of wthe ind turbine reduced when the SG speed increased above the rated power, and vice versa.

In a more recent study, Sharma *et al.* (2021) [25] evaluated the performance of CPSS and MB-PSS for the integration of 9 MW wind farm with a hydro power plant connected to 200 MVA power grid. The research demonstrated the superiority of MB-PSS over CPSS in improving the voltage profile and mitigating the effects of the faults. The results concluded that MB-PSS generated more active power at the output compared to CPSS.

In [26], researchers considered a standard IEEE system to analyze the transient stability with photovoltaic and wind energy. The results showed improved transient stability with the implementation of PSS4C but without optimization. In our previous work [7], an optimized MB-PSS4C was implemented to enhance the stability of the power system network with wind energy. Pattern search algorithm and simplex search algorithm were proposed to optimize the gains of the controller MB-PSS4C, then compared its performance with PSS1A. The results showed that the oscillation suppression with the optimized MB-PSS4C. However, the pattern search and simplex search methods are limited due to the need for users to define the initial parameters of MB-PSS4C before optimization. The limitation of these two methods motivated us to apply PSO, which can optimize the parameters randomly. Then, the parameters are updated for each iteration until the convergence solution is achieved.

To highlight the research gap, Table 1 summarizes the methodology and the findings from different research work. Moreover, it also compares the previous work with the current work. In view of the above, there is a considerable amount of research concerning the eigenvalue analysis and damping ratio analysis under different operating conditions to tune PSS parameters [13], [15], [27], [28]. Eigenvalue and damping ratio analysis are applied to linear power systems during a small-disturbance stability analysis, and they do

not reflect the dynamic performance of the power system accurately. Furthermore, a linearized approach for a large power system is a challenge to achieve, since the power systems are nonlinear in nature. The integration of wind energy into the system makes the linearization approach more complicated. Moreover, MB-PSS4C supersedes the PSS4B controller introduced in IEEE Std 421.5^{TM}-2005, and the time constants of second and third lead-lag filters are not specified in the IEEE Std 421.5^{TM}-2016 [29]. In this work, a new method is proposed to tune the parameters of MB-PSS4C using PSO.

Thus, the importance to suppress different oscillation modes and the need to select the parameters of PSS4C have propelled the importance to focus on the optimized MB-PSS4C. This research presents the implementation of the two-area system with four machines integrated with wind energy, and the power system stability is analyzed during the fault. The key contributions of this paper are summarized as follow:

1) Proposed an efficient method which is suitable for nonlinear power systems and applied this method to optimize the parameters of MB-PSS4C using PSO.
2) Compared the performance of Pattern Search (PS-MB-PSS4C) and Simplex Search (SS-MB-PSS4C) algorithms (from previous work) with PSO-MB-PSS4C to assess the efficacy of the proposed algorithm.
3) Verified the results of PSO-MB-PSS4C by comparing them with the performance of PSS1A, where parameters of PSS1A are chosen from IEEE standard 421.5^{TM}.
4) Investigated the effect of wind energy integrated into the network, where the SGs are equipped with MB-PSS4C.

This paper is structured as follows: Section II gives an overview of the mathematical models and the PSSs, formulation of the optimization method, and the electrical power systems; Section III describes the results of the method applied to the standard power system for the evaluation of its performance, followed by discussion and conclusion.

II. METHODOLOGY

There are several factors to be considered in the power system design which affect the spinning motion of the SGs. These factors include parameters of SGs, excitation systems, and operating conditions [30]. For instance, the excitation system functions to adjust the field current and maintain the appropriate generated voltage [26]. PSS is integrated with an excitation system to improve the power system stability, and it introduces an auxiliary signal to increase the damping of power system oscillations [10], [17].

Previous studies [7], [32] reported that the exciter ST1A integrated with PSS yields better performance than DC1A and IEEE Type 1. Therefore, the ST1A excitation system is implemented based on IEEE Std 421.5^{TM}-2005. Table 2 shows the data of the ST1A excitation system with a transient gain reduction [20]. Fig. 1 presents the research methodology that is implemented to optimize the parameters of PSO-MB-PSS4C to enhance the transient stability of power systems.

TABLE 1. Comparison of the existing work with the proposed work.

Reference	Controller used	Optimization Approach	Remarks
Khodabakhshian, Hemmati and Moazzami (2013) [19].	MB-PSS	culture-PSO-co-evolutionary (CPCE) algorithm	Proposed design suppressed the oscillations under different operating conditions
Rimorov, Kamwa, and Joós (2015) [13]	PSS4B	Improved Modal Performance Index	Presented method dampened different oscillation modes
Didier and Leveque (2016) [10]	PSS, MB-PSS, and superconducting fault current limiter	optimal location of superconducting fault current limiter	Angular separation variation of SG was mitigated
Bhukya and Mahajan (2019) [4]	PSS and SSSC	Eigenvalue analysis and PSO	Stability was enhanced and capability of machines was improved
Bhukya and Mahajan (2020) [14]	PSS, STATCOM, and SVC	Eigenvalue analysis and PSO	Linearization of nonlinear system was performed to analyze small-signal stability
Alsakati, Vaithilingam, Naidu, *et al.* (2021) [31]	PSS1A	PSO	PSO was applied to single-input PSS1A.
Huang *et al.* (2020) [23]	MB-PSS	An advanced closed-loop control	Frequency stability was enhanced and dampened the oscillation modes
Peres and da Costa (2020) [15]	STATCOM and MB controller	Eigenvalue and damping ratio analysis	The study recommended the use of active power in analyzing the stability of renewable energy integrated power system
Sharma *et al.* (2021) [25]	MB-PSS and CPSS	-	MB-PSS generates more active power than CPSS
Li, Tiong, and Wong (2019) [26]	PSS4B, PSS4C	-	PSS4C optimization was not available.
Alsakati *et al.* (2021a) [7]	PSS, MB-PSS4C	Simplex Search, and Pattern Search	Need for users to define initial values of MB-PSS4C for the application of the optimization methods.
The current research	PSS1A, MB-PSS4C	PSO	Comparison of the results of three optimization approaches Integrate different wind energy penetrations.

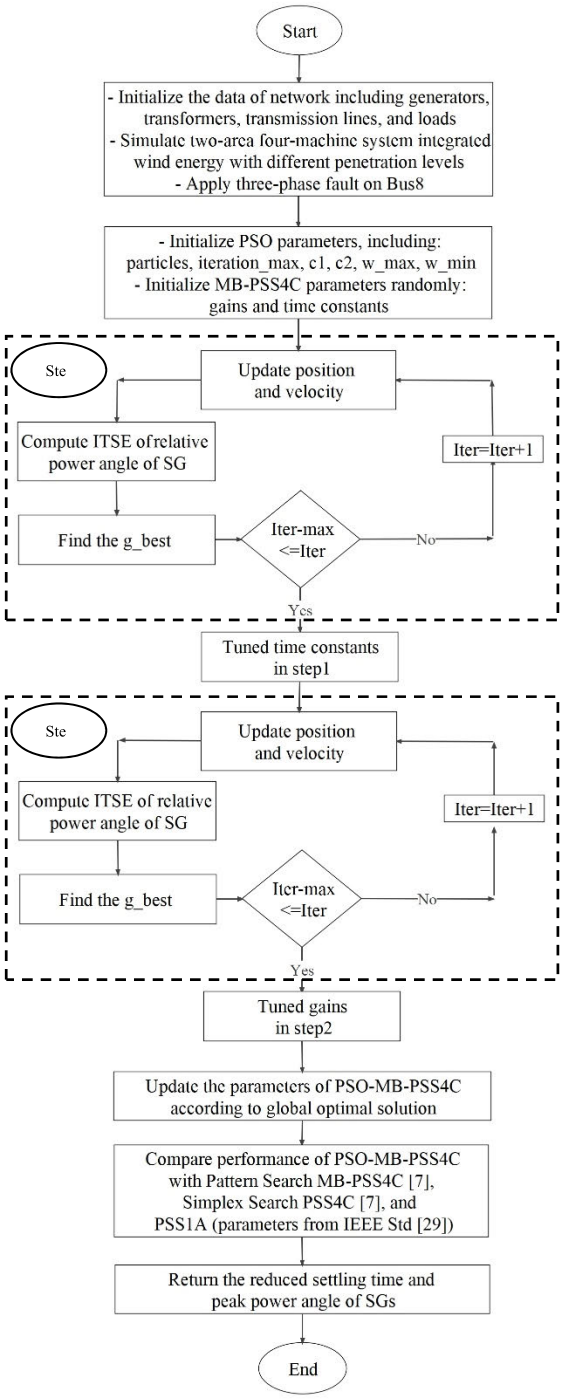

FIGURE 1. Flowchart of research methodology to optimize PSO-MB-PSS4C.

A. SYSTEM MODEL

An electrical power system with multi-machine uses a non-linear differential equation, described in Equation (1) [19]:

$$\dot{y} = f(y, x) \tag{1}$$

TABLE 2. Sample data for ST1A excitation system [20] *(IEEE 421.5-2005 - Adapted and reprinted with permission from IEEE. Copyright IEEE 2005. All rights reserved)*.

Parameters	Value	Parameters	Valu e
Low-pass filter time constant T_R s	0.04	Regulator denominator time constant T_{B1} s	0
Gain of voltage regulator Ka pu	190	Time constant of damping filter Tf s	1
Regulator numerator time constant T_C s	1	Rectifier loading factor K_C pu	0.08
Regulator denominator time constant T_B s	10	Exciter output current limiter gain K_{LR} pu	0
Regulator numerator time constant T_{C1} s	0	Exciter output current limit reference I_{LR} pu	0

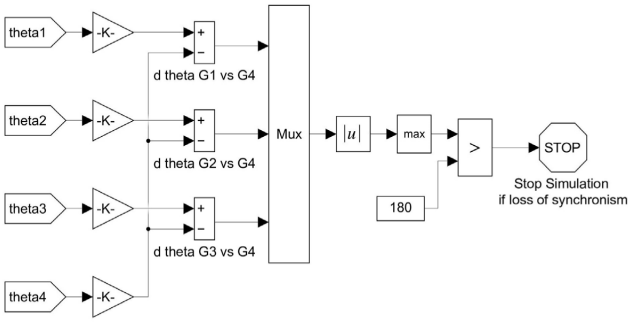

FIGURE 2. Transient stability limit designed in MATLAB/Simulink [37].

where y denotes the state variables, such as the rotor angle, speed, and voltage; x is the input control signal, which represents the PSS signal.

Meanwhile, Equation (2) represents the non-linear dynamic model for generator i [33], and the latter is used for the transient stability analysis:

$$\frac{H_i}{\pi f}\frac{d^2\delta_i}{dt^2} = P_{mech,i} - P_{e,i} \tag{2}$$

where δ_i is the power angle of the machine; P_{mechi} refers to mechanical input power; H_i denotes the inertia constant of the SG. The swing equation (2) is often used in transient stability studies, and it shows that the value of power angle is a function of the balance between mechanical and electrical power. If any change happens in the system, the balance is affected, and the power angle oscillates and moves to other positions.

Equations (3), (4) [33] and Equation (5) [27] evaluates the internal transient voltages ($E'_{q,i}$, $E'_{d,i}$), and field voltage $E_{fd,i}$ of SG i:

$$\frac{dE'_{q,i}}{dt} = \frac{1}{T'_{d0,i}}(E_{fd,i} - E'_{q,i} - i_{d,i}(x_{d,i} - x'_{d,i})) \tag{3}$$

$$\frac{dE'_{d,i}}{dt} = \frac{1}{T'_{q0,i}}(-E'_{d,i} - i_{q,i}(x_{q,i} - x'_{q,i})) \tag{4}$$

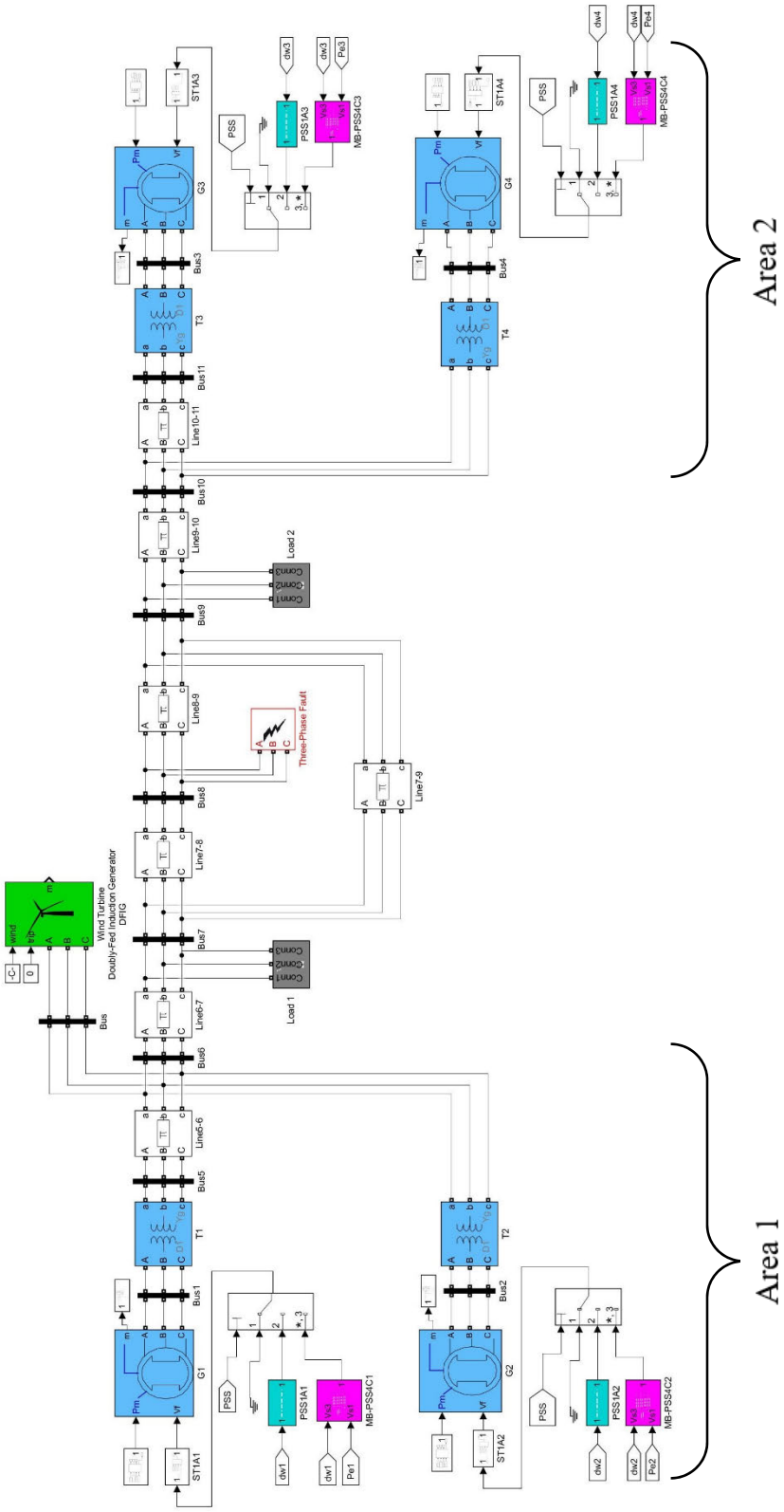

FIGURE 3. Diagram of two-area four-machine system integrated wind energy, subjected to a three-phase fault in Bus8. (parameters of the existing system are found in [34], [37]).

$$E_{fd,i} = \frac{1}{T_{a,i}}(-E_{fd,i} + K_{a,i}(V_{ref,i} + V_{PSS,i} - V_{t,i})) \quad (5)$$

where $x_{d,i}$ and $x'_{d,i}$ are d-axis reactance and transient reactance. While, $x_{q,i}$ and $x'_{q,i}$ are q-axis reactance and transient reactance. $T'_{d0,i}$ and $T'_{q0,i}$ are the time constant of SG i on d-q axis.

MATLAB/Simulink is used to model the electrical network, tune PSS parameters, and analyze system stability. As part of the proposed method to improve system stability, PSS1A and MB-PSS4C are modeled and evaluated to assess the stability performance under large disturbances. There are several factors to be considered in the evaluation of transient stability, such as the relative power angle [7], [10], [28], [30], [32], [34], power angle [9], speed deviation [32], [35], rotor speed [4], [14], and electrical power of SGs [14], [28], [36].

Transient stability, as described in the introduction, is the ability of SGs to maintain synchronism when subjected to a larger disturbance. Power angle differences and speed deviation of SGs are used as generator stability indicators. A decrease in the relative power angle indicates a stable system. In contrast, when the relative power angle of SG increases to a large value, the generator loses synchronism which leads to system instability [7], [30], [34]. The power angle of SG based on reference generator is represented by Equation (6) [30]:

$$\delta_{i,ref} = \delta_i - \delta_{ref} \quad (6)$$

where δ_i is the power angle of a generator; δ_{ref} is the power angle of the reference; $\delta_{i,ref}$ is the power angle differences between each generator and reference generator in degree. The system is considered transient stable if all SGs reach steady-state condition after disturbance. The transient stability limit for any synchronous generator is when the relative power angle (power angle difference) is less than 180° (π radians) [30], [37]. Fig. 2 shows the transient stability limit designed in MATLAB/Simulink, where the system loses its stability if the relative power angle exceeds the limit [37].

Wind Energy Model: The wind generator converts the mechanical power to electrical power as it extracts from Equation (7) injected into the turbine [38]:

$$P_{wind} = \frac{1}{2}\rho \cdot A \cdot V^3 \quad (7)$$

where V is the wind speed; A is the swept area of the turbine; ρ is the air density.

The electrical output of the generator produced by wind energy conversion system is presented by Equation (8) [38]–[40] with the practical limitations of the proven Betz limit [41].

The power coefficient, C_P, is given by Equation (9) [38], [39], where C_P correlates with the blade angle, tip speed ratio λ (given by Equation (10)), and speed of wind, V.

$$P_{out} = \frac{1}{2}\rho \cdot A \cdot C_P \cdot V^3 \quad (8)$$

$$C_P = f(\lambda, \beta) \quad (9)$$

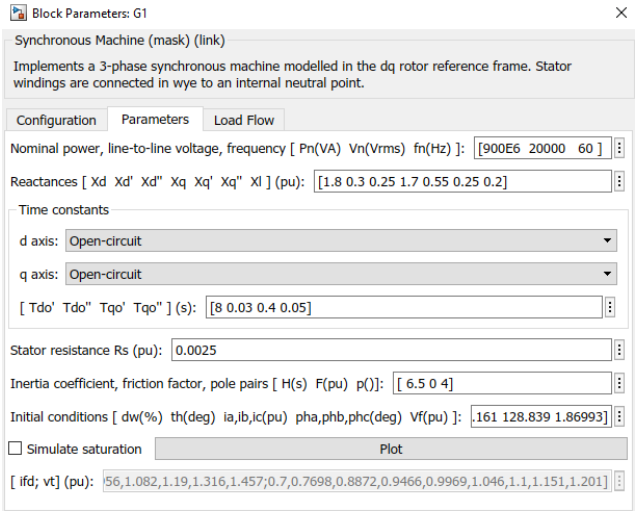

FIGURE 4. Generator parameters include capacity, reactance, and d-q axis time constants of SGs. Inertia coefficient $H = 6.5$ s (for G1 and G2), $H = 6.175$ (for G3 and G4) [34], [37].

$$\lambda = \frac{R * w_R}{V} \quad (10)$$

B. TWO-AREA FOUR-MACHINE SYSTEM

This work selects a specific system to investigate power system oscillations in the interconnected power system. This system comprises two areas connected by 230 kV transmission network as well as two constant loads connected to Bus7 and Bus9. These two areas are equipped with SGs with a rating of 900 MVA/20 kV. Fig. 3 presents the structure of the system used in this research, which is integrated with the PSS and wind energy, and simulated by the MATLAB/Simulink. To investigate the effect of wind energy on transient stability, wind turbines are connected to the existing system on Bus6. The location of wind energy is selected from the literature [7] for other optimization methods validations.

The generator parameters are given in Fig. 4, where the reactances are in per unit, and d-q axis time constants are in seconds [34], [37]. SGs are integrated with the governor, excitation system type ST1A, and PSS. The frequency of the system is 60 Hz. The current work referred to the literature [34], [37] to determine the parameters of SGs, transformers, lines, and loads. The parameters of transmission line in per unit are $r = 0.0001$ pu/km, $x_L = 0.001$ pu/km, and $b_C = 0.00175$ pu/km. Load are connected to Bus7 & and Bus9. The load and reactive power supplied by capacitors at Bus7 are $P_L = 967$ MW, $Q_L = 100$ MVAr, and $Q_C = 200$ MVAr. While at Bus 9, the load and Q_C are $P_L = 1,767$ MW, $Q_L = 100$ MVAr, and $Q_C = 350$ MVAr.

A three-phase fault occurs at Bus8; the fault then self-clears in 12 cycles (200 ms). With different wind energy penetrations, the effects of Double Fed Induction Generators (DFIGs) on transient stability are analyzed. DFIGs present a good performance in reducing the relative power angle of SGs [42]. In particular, with reference to [7], three

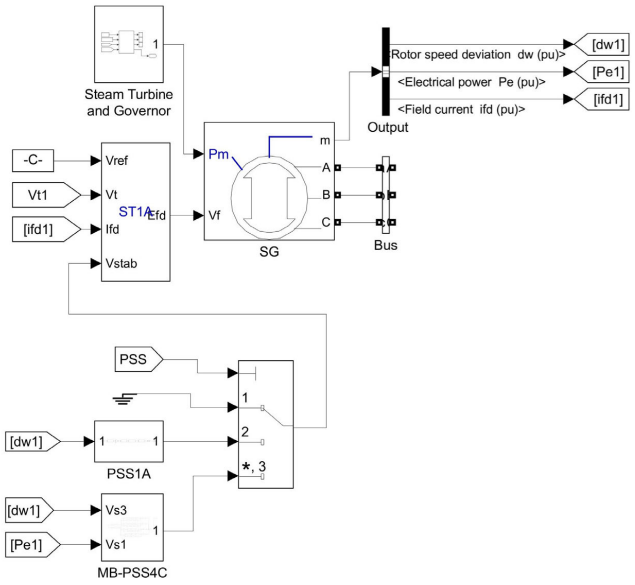

FIGURE 5. Synchronous generator is connected to the network and equipped with excitation system, governor and different types of PSSs.

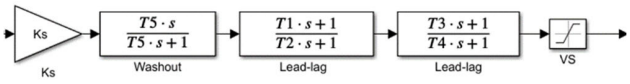

FIGURE 6. Diagram of PSS1A with speed deviation input.

wind energy penetration levels, specifically 36 MW (considered as low penetration wind energy, where the system is stable), 72 MW, and 108 MW (considered as high penetration due to the significant increase in the settling time of relative power angles), are selected for this research in order to compare the performance of PSO with the simplex search and pattern search optimization methods.

The input of PSS1A is the speed deviation of SG, while the inputs of MB-PSS4C are speed deviation and electrical power of SG. Power system stabilizer produces a signal to control the excitation system. The speed govern and excitation system adjust the electrical power and terminal voltage of SG. Fig. 5 illustrates the diagram of the control systems connected to the synchronous generator, and it also includes the connection of two types of PSSs to the system.

1) SINGLE-INPUT PSS1A

Fig. 6 illustrates the PSS diagram with single input and its components. The washout high-pass filter is used to keep the controller output at zero under steady-state conditions [16] and to enable the frequency ranges to pass during a transient period [5]. Meanwhile, the signal is limited from exceeding specific values by the limiter. PSS input signal serves as the speed deviation, while its output indicates the input of the exciter. The parameters of PSS1A, including gain and time constants, are selected according to the type of excitation system applied. The sample data of PSS-integrated ST1A is based on the IEEE standard [29].

2) MULTI-AND PSS4C

In this research, the MB-PSS4C is implemented, which supersedes the PSS4B controller introduced in IEEE recommended practice 2005 [29]. Fig. 7 shows the block diagram for MB-PSS4C [29]. MB-PSS4C combines the speed deviation of SG, dw, and electrical power, P_e. Besides that, it consists of multiple frequency bands. The parameters of MB-PSS4C can be found in IEEE standard [29].

The need for efficient damping of different electromechanical modes led to the development of MB-PSS4C, which uses four bands to dampen the power system disturbances for different frequency modes. Referring to Equations (11–14) [29], [43], time constants of first lead-lag filters can be calculated for the high-band mode. Using these equations, it is possible to derive time constants of first lead-lag filters for other band modes taking into consideration the following frequency bands: $F_{VL} = 0.01$ Hz; $F_L = 0.07$ Hz; $F_I = 0.6$ Hz, and $F_H = 9$ Hz, and R equals to 1.2 [29].

$$T_{H2} = \frac{1}{2\pi * F_H * \sqrt{R}} \tag{11}$$

$$T_{H1} = \frac{T_{H2}}{R} \tag{12}$$

$$T_{H7} = T_{H2} \tag{13}$$

$$T_{H8} = R * T_{H7}$$

$$T_{H2} = T_{H7} = \frac{1}{2\pi * 9 * \sqrt{1.2}} = 0.01614\,\text{sec}$$

$$T_{H1} = \frac{0.01614}{1.2} = 0.01345\,\text{sec}$$

$$T_{H8} = 1.2 * 0.0161 = 0.01937\,\text{sec} \tag{14}$$

However, the time constants of the second and third lead-lag filters are zero by default, based on IEEE standard [29]. In this work, the optimization approach is implemented to tune the gains and time constants of the second and third lead-lag filters for optimal performance.

C. PARTICLE SWARM OPTIMIZATION (PSO)

A concept of optimization for nonlinear functions was introduced in 1995 [44]. Particle Swarm Optimization (PSO) is inspired by the behavior of social groups, including fish schooling and bird flocking. It is a common algorithm that is used to optimize the PSS controller, where the solutions are achieved without considering the initial population, and the balance of the local and global search space are controlled [45]. The population (swarm) is initialized randomly, and the generations are updated through iterations to find the optimal solution. PSO uses the local search and global search optimization methods, attempting to balance exploration. The local search method represents the self-experience, while the global search represents the neighboring experience [46].

In this work, the method starts by initializing gains and time constants of the controller, inertia weight, and acceleration factors. The lower and upper bounds (constraints) of parameters are specified using the trial and error method. The objective function of the integral time squared error

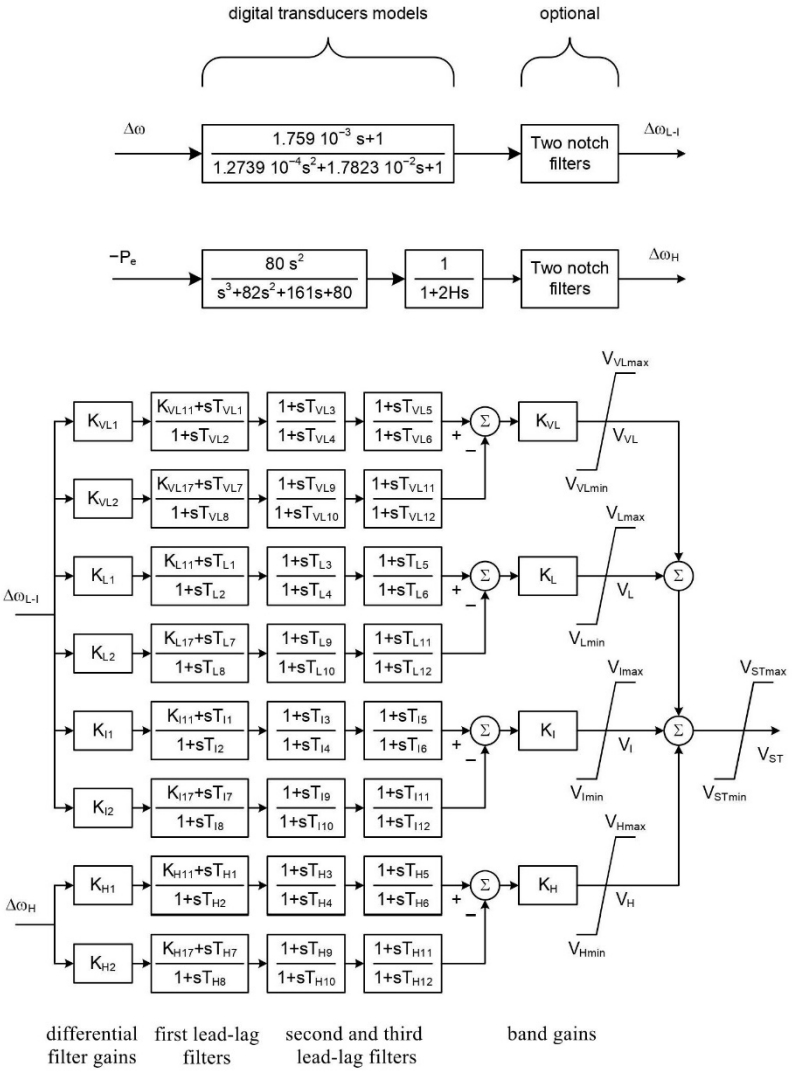

FIGURE 7. **Diagram of MB-PSS4C modeled in MATLAB [29].** ***(IEEE 421.5-2016 - Reprinted and adapted with permission from IEEE. Copyright IEEE 2016. All rights reserved).***

minimizes the relative power angle of SG, as in Equation (15). The particles move to a new position using their velocity, based on the best experience, local best, *P_best* (position of a particle). *G_best* (global best) is the best value, in the population achieved by all particles. The velocity and position of each particle are modified for each iteration using Equation (16) and Equation (17) [45], [47]. The modification of each iteration is based on the data of the current position, *P_best*, and *G_best*.

$$ITSE = \int t.\delta^2.dt \tag{15}$$

$$v_{ia}^{(iter+1)} = w_{updated} * v_{ia}^{(iter)} + r1 * c1 * (p\_best_{ia} - x_{ia}^{(iter)}) + r2 * c2 * (g\_best_{ia} - x_{ia}^{(iter)}) \tag{16}$$

$$x_{ia}^{(iter+1)} = x_{ia}^{(iter)} + v_{ia}^{(iter+1)} \tag{17}$$

where the number of iterations is *iter*, the velocity of each particle $v_{ia}^{(iter)}$, and the position of particle $x_{ia}^{(iter)}$ at iteration *iter*. $c1 = 2$ and $c2 = 2$ are the acceleration factors, and *r1* and *r2* are random values, while *w* is inertia weight.

The use of linear decrease of the inertia weight shows better improvement in the applications. Equation (18) calculates the value of updated inertia weight [48]:

$$w_{updated} = w_{\max} - \frac{w_{\max} - w_{\min}}{iteration_{\max}} * iteration \tag{18}$$

where $iteration_{max}$ is the maximum iteration, and *iteration* is the current iteration; w_{max} and w_{min} are 0.9 and 0.4, respectively.

MB-PSS4C consists of large numbers of parameters with multiple transfer functions and Equations (11–14) determine the time constants of the first lead-lag filters. Therefore, the parameters of the first lead-lag filters are kept similar to the typical data used in IEEE standard [29]. In this study, the rest of MB-PSS4C parameters are optimized using the PSO method. The parameters are tuned using two steps, the first

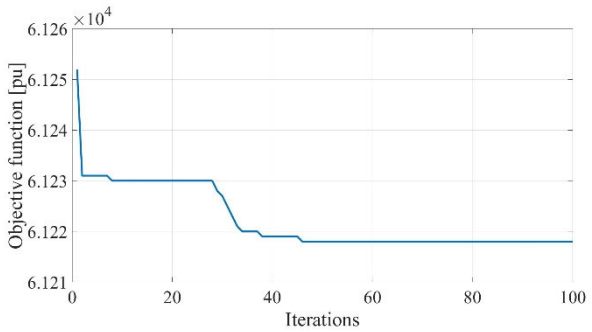

FIGURE 8. Convergence performance for power angle minimization to optimize the gains of MB-PSS4C in step2.

step is to optimize the time constants of second and third lead-lag filters. While, the optimization of gains is achieved in the second step. The constraints for each band are defined to ensure the gain and time constant limitations, as in Equations (19-29), for very low band.

$$T_{VL3(\min)} \leq T_{VL3} \leq T_{VL3(\max)} \quad (19)$$
$$T_{VL4(\min)} \leq T_{VL4} \leq T_{VL4(\max)} \quad (20)$$
$$T_{VL5(\min)} \leq T_{VL5} \leq T_{VL5(\max)} \quad (21)$$
$$T_{VL6(\min)} \leq T_{VL6} \leq T_{VL6(\max)} \quad (22)$$
$$T_{VL9(\min)} \leq T_{VL9} \leq T_{VL9(\max)} \quad (23)$$
$$T_{VL10(\min)} \leq T_{VL10} \leq T_{VL10(\max)} \quad (24)$$
$$T_{VL11(\min)} \leq T_{VL11} \leq T_{VL11(\max)} \quad (25)$$
$$T_{VL12(\min)} \leq T_{VL12} \leq T_{VL12(\max)} \quad (26)$$
$$K_{VL(\min)} \leq K_{VL} \leq K_{VL(\max)} \quad (27)$$
$$K_{VL1(\min)} \leq K_{VL1} \leq K_{VL1(\max)} \quad (28)$$
$$K_{VL2(\min)} \leq K_{VL2} \leq K_{VL2(\max)} \quad (29)$$

This method minimizes the relative power angle of SG without the need to specify the initial value of the parameters. Band gains, differential filter gains, and time constants for second lead-lag and third lead-lag filters are selected to tune PSO-MB-PSS4C (the filters are illustrated in Fig. 7). Table 3 shows the tuned gains and time constants of PSO-MB-PSS4C using the PSO method. Integral Time Squared Error is the objective function used to tune MB-PSS4C's gains (step2), as shown in Fig. 8.

III. RESULTS AND DISCUSSION

A. TRANSIENT STABILITY ANALYSIS

In this study, the transient stability of the system is assessed during a three-phase fault occurring at Bus8. Referring to Fig. 9, the results illustrate that the power angle differences of the SGs oscillate. Furthermore, the relative power angle $\delta_{1,4}$ of Generator1 is found to be higher than the relative power angle of other generators. Therefore, the following figures and results focus on the transient stability assessment of Generator1. Fig. 10 illustrates the speed deviations of SGs, in which all generators oscillate, whereby the system is found

TABLE 3. Tuned parameters of PSO-MB-PSS4C integrated into the studied system.

Parameters	Value	Parameters	Value
T_{VL3}	0.5673	T_{I11}	0.15
T_{VL4}	0.0253	T_{I12}	0.03
T_{VL5}	1	T_{H3}	0.15
T_{VL6}	0.0299	T_{H4}	0.03
T_{VL9}	0.9182	T_{H5}	0.15
T_{VL10}	0.0222	T_{H6}	0.03
T_{VL11}	0.7511	T_{H9}	0.15
T_{VL12}	0.0193	T_{H10}	0.03
T_{L3}	0.1828	T_{H11}	0.15
T_{L4}	0.0287	T_{H12}	0.03
T_{L5}	0.1953	K_{VL}	0.1
T_{L6}	0.0208	K_{VL1}	81.4106
T_{L9}	0.15	K_{VL2}	50
T_{L10}	0.0351	K_L	0.1
T_{L11}	0.15	K_{L1}	66
T_{L12}	0.03	K_{L2}	66
T_{I3}	0.15	K_I	20
T_{I4}	0.03	K_{I1}	66
T_{I5}	0.15	K_{I2}	65
T_{I6}	0.03	K_H	50
T_{I9}	0.15	K_{H1}	66
T_{I10}	0.03	K_{H2}	66

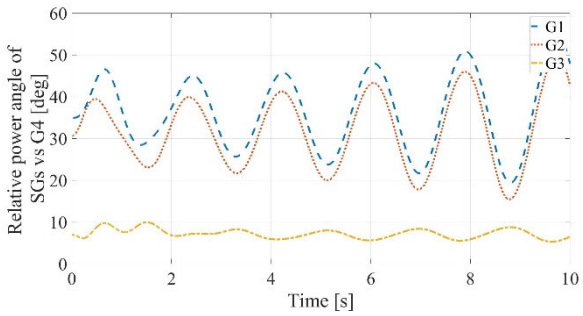

FIGURE 9. Power angle differences of generators based on Generator4 for the studied system without PSS.

to be unstable. As shown in Fig. 11, similar observations are found through the active power of SGs affected by the disturbance. Thus, an extra controller is necessary to increase the stability of the system.

1) TRANSIENT STABILITY ANALYSIS OF THE SYSTEM EQUIPPED WITH PSS

This subsection discusses the power system stability of the studied system during the fault. The power angle differences of SG is selected to evaluate the system stability. Four different cases are investigated and compared to identify the suitable design of PSS. Accordingly, the gain and time constants of PSS1A are selected from IEEE standard [29]. Meanwhile,

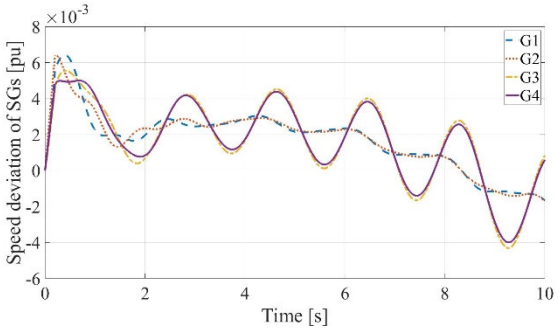

FIGURE 10. Speed deviation of generators for the system without PSS.

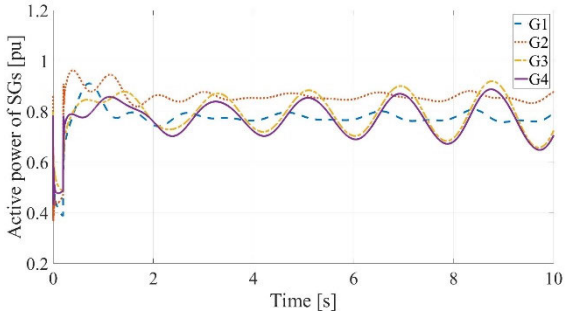

FIGURE 11. Active power of generators, for the system before adding PSS.

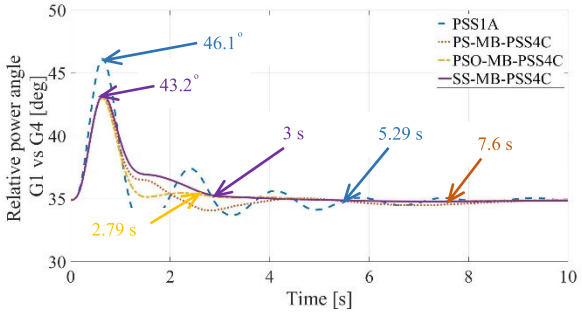

FIGURE 12. Performance of different optimization methods considering Generator1 $\delta_{1,4}$, The studied system without wind energy.

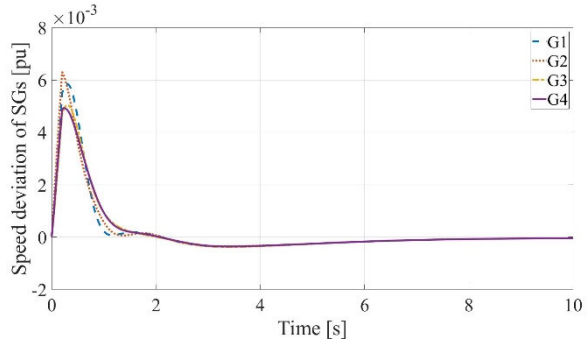

FIGURE 13. Speed deviation of generators, The studied system equipped with PSO-MB-PSS4C.

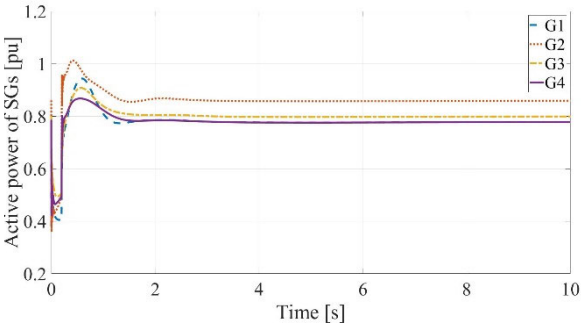

FIGURE 14. Active power of generators, The studied system equipped with PSO-MB-PSS4C.

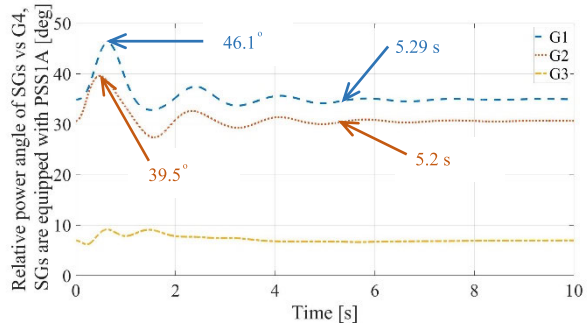

FIGURE 15. Power angle differences of generators based on Generator4 where SGs are equipped with PSS1A.

Pattern Search-MB-PSS4C (PS-MB-PSS4C)'s parameters are tuned using the pattern search method, whereas Simplex Search-MB-PSS4C (SS-MB-PSS4C) is tuned based on simplex search. This research selects the parameters of PS-MB-PSS4C and SS-MB-PSS4C from our previous work [7]. On the other hand, the parameters of PSO-MB-PSS4C are tuned using PSO method.

Fig. 12 compares the performance of different PSS optimization methods. MB-PSS4C recorded similar results in terms of peak power angle, where the peak value is recorded around 43.2°. In addition, the settling time of PS-MB-PSS4C is around 7.6 s, which is 60.5% higher than the settling time recorded by SS-MB-PSS4C at 3 s. However, the implementation of PSO-MB-PSS4C records the shortest settling time at 2.79 s.

Meanwhile, Fig. 13 shows the speed deviation of SGs when PSO-MB-PSS4C is utilized. The obtained results reveal constant speed deviation for all SGs during a shorter period. Moreover, as shown in Fig. 14, the active power output of SGs improve after the implementation of PSO-MB-PSS4C, as compared to the fluctuating power output presented in Fig. 11. In other words, the active power waveforms remain constant after the first swing.

Figure 15 to Figure 18 present the power angle differences (relative power angle) of synchronous generators (G1, G2, and G3) with respect to the reference generator, G4. Additionally, a comparison of the performance of different optimization methods on the transient stability enhancement

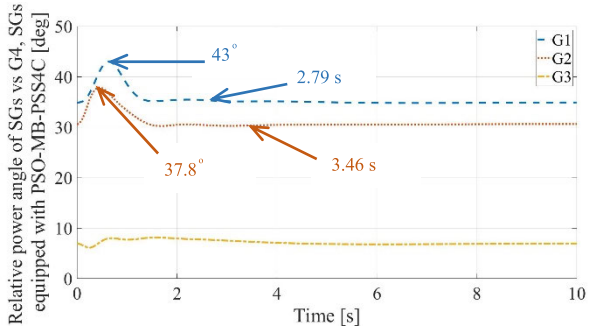

FIGURE 16. Power angle differences of generators based on Generator4 where SGs are equipped with PSO-MB-PSS4C.

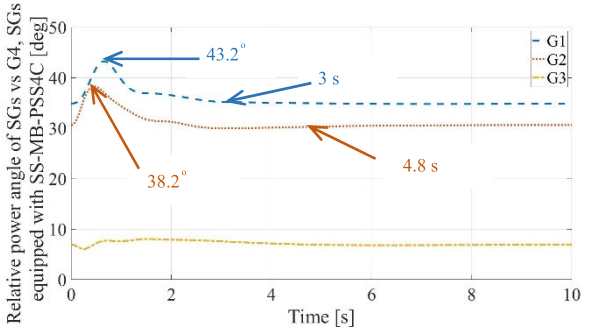

FIGURE 17. Power angle differences of generators based on Generator4 where SGs are equipped with SS-MB-PSS4C.

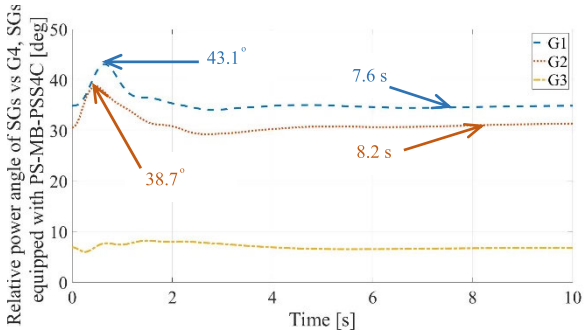

FIGURE 18. Power angle differences of generators based on Generator4 where SGs are equipped with PS-MB-PSS4C.

is presented. Fig. 15 shows the power angle difference of SGs with respect to G4, where the SGs are equipped with PSS1A. The settling time for both G1 and G2 is around 5s, while the power angle of G3 remains constant. The optimized MB-PSS4C based on PSO (PSO-MB-PSS4C) records the shortest settling time and the lowest power angle of SGs compared with simplex search (SS-MB-PSS4C) and pattern search (PS-MB-PSS4C) optimization methods, as presented in Fig. 16, Fig. 17 and Fig. 18 respectively. Generator 3 is stable because the changes in power angle are very small, and the peak value is less than 10°.

To verify the performance of PSO-MB-PSS4C, the three-phase faults are tested individually and applied to different locations within the transmission network. Fig. 19 shows the relative power angle of G1 when the fault occurs at different buses (Bus 5 - Bus 11), respectively. As observed, the peak power angle increases when the fault occurs near an SG. However, the system equipped with PSO-MB-PSS4C remains stable in all cases. Table 4 compares the results of the power angle for different fault locations. The fault on Bus8 has a small impact on the system, but the fault on Bus6 has the highest effect on the system, where the power angle indicates an increase to126.37°, then remain to stability after 4.41 s.

TABLE 4. Transient stability analysis when fault occurs on different locations.

Fault on Bus	Settling Time in s	Max Value of $\delta_{1,4}$°
Bus5	3.54 s	106.85°
Bus6	4.41 s	126.37°
Bus7	2.81 s	100.96°
Bus8	2.79 s	43.00°
Bus9	3.68 s	59.64°
Bus10	3.79 s	72.27°
Bus11	5.04 s	81.60°

2) TRANSIENT STABILITY ANALYSIS OF THE INTEGRATION OF WIND ENERGY

This subsection analyzes the effects of wind penetration on the transient stability of the studied system. Various wind energy penetrations, from 36 MW (low penetration) to 108 MW (high penetration), are selected from previous work [7]. The results revealed improved transient stability with the implementation of PSS1A and MB-PSS4C. As shown in Fig. 20, it is worth noting that the peak value of $\delta_{1,4}$., 43.45°, is almost like the existing system (without wind energy). Meanwhile, the settling time of $\delta_{1,4}$ is reduced to 1.36 s with the wind energy capacity that equals to 36 MW. As compared to other methods, PSO-MB-PSS4C presents a better performance. On the other hand, the settling time of $\delta_{1,4}$ is extended to more than 7s with high wind penetration, as illustrated in Fig. 21 and Fig. 22. In other words, wind energy with a large capacity, affects the power system's stability, and increases the settling time of relative power angle.

To validate these results and determine the maximum wind penetration that could be injected with the lowest settling time, several penetration levels ranging from 36MW to 108 MW are tested. Table 5 compares the power angle differences of Generator1 with the integration of different wind energy penetrations together with other optimization methods reported from previous work [7] (Simplex Search and Pattern Search). The results reveal an approximately constant peak power angle for all penetration levels.

However, the connection of 48 MW wind energy shows a low value of settling time. The implementation of PSO-MB-PSS4C and SS-MB-PSS4C recorded the settling time of 1.35 s and 2.64 s, respectively. With that, these results

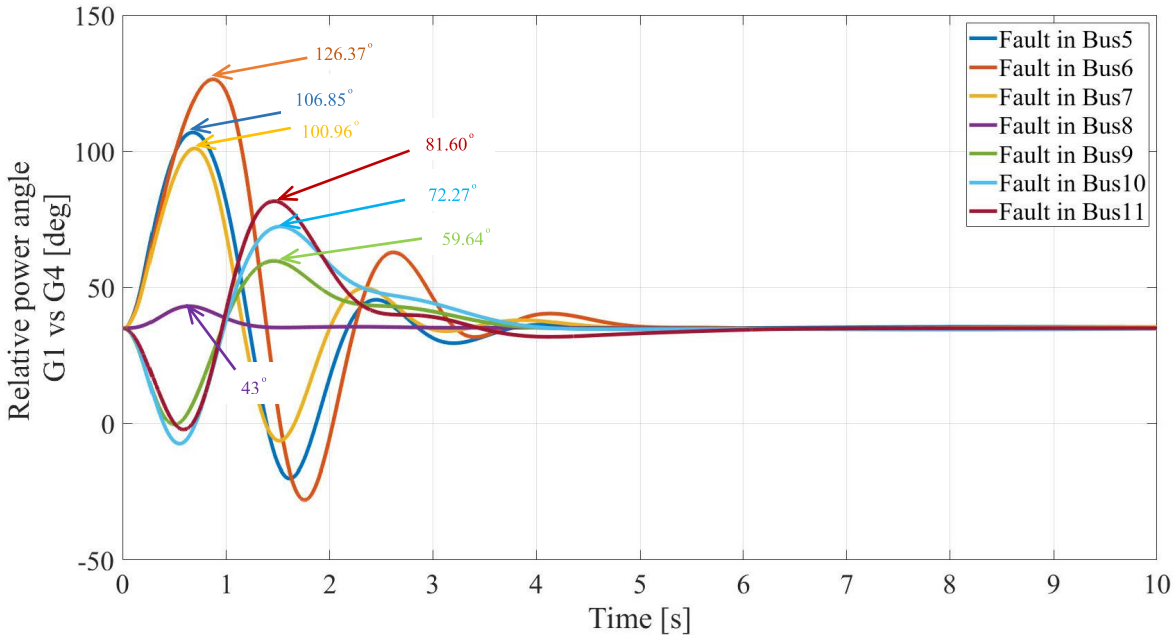

FIGURE 19. Power angle differences of Generator1 based on Generator 4 when faults occur on different busses, SGs are equipped with PSO-MB-PSS4C.

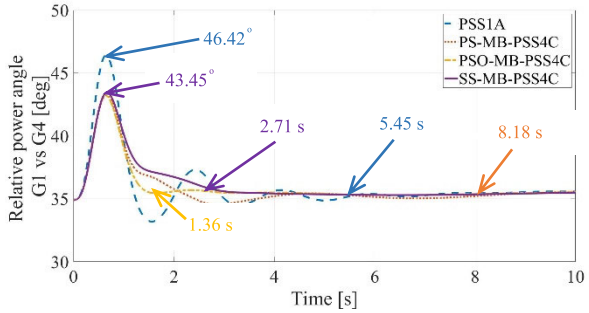

FIGURE 20. Performance of different optimization methods considering $\delta_{1,4}$ relative power angle. Studied system with 36 MW based wind energy.

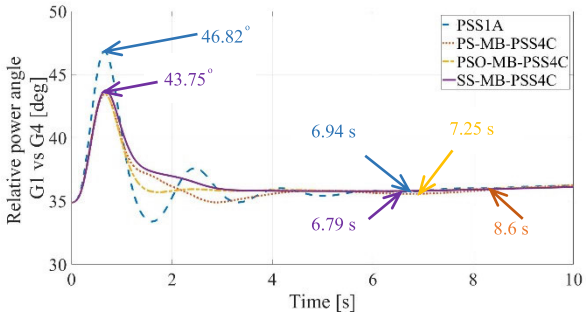

FIGURE 21. Performance of different optimization methods considering $\delta_{1,4}$ relative power angle. Studied system with 72 MW based wind energy.

conclude that 48 MW wind energy is a good option for the studied system to reduce the power angle differences and settling time.

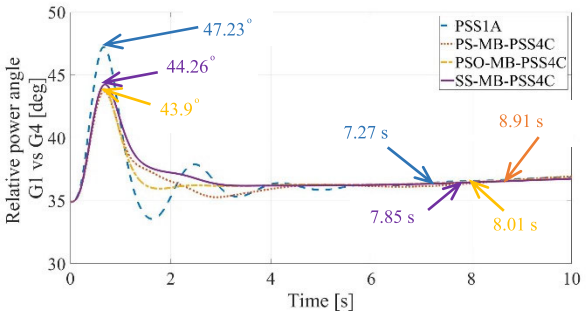

FIGURE 22. Performance of different optimization methods considering $\delta_{1,4}$ relative power angle. Studied system with 108 MW based wind energy.

When analyzing wind energy's contribution towards the power system stability, it must be kept in mind that the capacity of wind energy will be a part of the total power system capacity. Therefore, when the wind energy capacity is selected accurately, the power of SGs and wind turbines contribute together to meet the loads. While wind energy with a larger rating will cause adverse effects on system stability (108 MW wind energy in this research). The generation is greater than load, and power angle of SGs increased. Hence, high wind energy is not recommended in this case.

IV. CONCLUSION

This work systematically evaluates the performance of PSS1A and MB-PSS4C, and the effect of PSSs on the transient stability for grid integrated wind energy. Although MB-PSS4C has many parameters, the PSO is proven to be an

TABLE 5. Compare the power angle $\delta_{1,4}$ for different optimization methods with the integration of wind energy.

Power Angle Differences	Type of Controller	System without Wind Energy	Wind Energy up to 36 MW	Wind Energy up to 48 MW	Wind Energy up to 72 MW	Wind Energy up to 108 MW
Settling Time s	Existing system	System Unstable	System Unstable	System Unstable	System Unstable	System Unstable
	PSS1A	5.29 s	5.45 s	5.55 s	6.94 s	7.27 s
	Pattern Search-MB-PSS4C [7]	7.6 s	8.18 s	8.34 s	8.6 s	8.91 s
	Simplex Search-MB-PSS4C [7]	3 s	2.71 s	2.64 s	6.79 s	7.85 s
	PSO-MB-PSS4C	2.79 s	1.36 s	1.35 s	7.25 s	8.01 s
Peak Value of $\delta_{1,4}^{\circ}$	Existing System	58.5 °	46.6	46.72 °	47.01°	49.2
	PSS1A	46.1°	46.42°	46.53°	46.82°	47.23°
	Pattern Search-MB-PSS4C [7]	43.1°	43.25°	43.24°	43.46°	43.68°
	Simplex Search-MB-PSS4C [7]	43.2°	43.45°	43.46°	43.75°	44.26°
	PSO-MB-PSS4C	43.00°	43.2 °	43.31°	43.55°	43.9°

effective method in tuning the controller for improved performance. PSO is implemented to identify the optimal MP-PSS4C parameters. The findings here prove the effectiveness of the tuning approach and the efficiency of PSO-MB-PSS4C, where oscillations are quickly damped out in comparison with other methods. In particular, the utilization of PSO-MB-PSS4C shows better performance in reducing settling time, whereby the settling time reduces from 3s (SS-MB-PSS4C) to 2.79s (PSO-MB-PSS4C), and the decrease in settling time is approximately 7%. The settling time reduces from 5.29s (PSS1A) to 2.79s (PSO-MB-PSS4C), and the decrease in settling time is around 47%. The integration of 48 MW wind energy also is an indication of improved stability and reduced the settling time to 1.35s. However, high wind penetration up to 108 MW has increased the settling time to around 8s.

In this research, the PSO approach is applied to optimize the parameters of MB-PSS4C and improve the transient stability of wind energy integrated power system. However, this current work does not include the optimization of wind turbines' locations.

The use of PSO to optimize MB-PSS4C could be considered as future work to enhance the transient stability of the hybrid solar and wind farms integrated power systems.

ACKNOWLEDGMENT

The authors would like to acknowledge the contributions of the National Energy Research Center (NERC), Ministry of Electricity in Syria, by providing the wind speed data in Qatineh project.

REFERENCES

[1] C. V. Aravind, M. Al-Atabi, J. Ravishankar, A. Malik, Arkar, and E. Ambikairajah, "Eco-tourism sustainability through PV technology: A comprehensive review," *J. Eng. Sci. Technol.*, vol. 8, no. 6, pp. 654–669, 2013.

[2] M. S. A. Khan, R. K. Rajkumar, C. V. Aravind, and Y. W. Wong, "Feasibility study of a novel 6V supercapacitor based energy harvesting circuit integrated with vertical axis wind turbine for low wind areas," *Int. J. Renew. Energy Res.*, vol. 6, no. 3, pp. 1167–1177, 2016.

[3] (Mar. 10, 2021). *Top 5 Fastest-Growing Renewable Energy Sources Around the World*. Accessed: Nov. 29, 2021. [Online]. Available: https://earth.org/fastest-growing-renewable-energy-sources/

[4] J. Bhukya and V. Mahajan, "Optimization of damping controller for PSS and SSSC to improve stability of interconnected system with DFIG based wind farm," *Int. J. Electr. Power Energy Syst.*, vol. 108, pp. 314–335, Jun. 2019, doi: 10.1016/j.ijepes.2019.01.017.

[5] M. Edrah, K. L. Lo, and O. Anaya-Lara, "Impacts of high penetration of DFIG wind turbines on rotor angle stability of power systems," *IEEE Trans. Sustain. Energy*, vol. 6, no. 3, pp. 759–766, Jul. 2015, doi: 10.1109/TSTE.2015.2412176.

[6] M. A. S. Ali, K. K. Mehmood, S. Baloch, and C.-H. Kim, "Modified rotor-side converter control design for improving the LVRT capability of a DFIG-based WECS," *Electr. Power Syst. Res.*, vol. 186, Sep. 2020, Art. no. 106403, doi: 10.1016/j.epsr.2020.106403.

[7] A. A. Alsakati, C. A. Vaithilingam, J. Alnasseir, and A. Jagadeeshwaran, "Simplex search method driven design for transient stability enhancement in wind energy integrated power system using multi-band PSS4C," *IEEE Access*, vol. 9, pp. 83913–83928, 2021, doi: 10.1109/ACCESS.2021.3085976.

[8] P. Kundur, J. Paserba, V. Ajjarapu, G. Andersson, A. Bose, C. Canizares, N. Hatziargyriou, D. Hill, A. Stankovic, C. Taylor, T. Van Cutsem, and V. Vittal, "Definition and classification of power system stability IEEE/CIGRE joint task force on stability terms and definitions," *IEEE Trans. Power Syst.*, vol. 19, no. 3, pp. 1387–1401, May 2004, doi: 10.1109/TPWRS.2004.825981.

[9] M. M. Eladany, A. A. Eldesouky, and A. A. Sallam, "Power system transient stability: An algorithm for assessment and enhancement based on catastrophe theory and FACTS devices," *IEEE Access*, vol. 6, pp. 26424–26437, 2018, doi: 10.1109/ACCESS.2018.2834906.

[10] G. Didier and J. Leveque, "Study of optimal combination between SFCL location and PSS type to improve power system transient stability," *Int. J. Electr. Power Energy Syst.*, vol. 77, pp. 158–165, May 2016, doi: 10.1016/j.ijepes.2015.11.007.

[11] T. Hussein, M. S. Saad, A. L. Elshafei, and A. Bahgat, "Damping inter-area modes of oscillation using an adaptive fuzzy power system stabilizer," *Electr. Power Syst. Res.*, vol. 80, no. 12, pp. 1428–1436, Dec. 2010, doi: 10.1016/j.epsr.2010.06.004.

[12] D. Cai, P. Regulski, M. Osborne, and V. Terzija, "Wide area inter-area oscillation monitoring using fast nonlinear estimation algorithm," *IEEE Trans. Smart Grid*, vol. 4, no. 3, pp. 1721–1731, Sep. 2013, doi: 10.1109/TSG.2013.2257890.

[13] D. Rimorov, I. Kamwa, and G. Joós, "Model-based tuning approach for multi-band power system stabilisers PSS4B using an improved modal performance index," *IET Gener., Transmiss. Distrib.*, vol. 9, no. 15, pp. 2135–2143, Nov. 2015, doi: 10.1049/iet-gtd.2014.1176.

[14] J. Bhukya and V. Mahajan, "Optimization of controllers parameters for damping local area oscillation to enhance the stability of an interconnected system with wind farm," *Int. J. Electr. Power Energy Syst.*, vol. 119, Jul. 2020, Art. no. 105877, doi: 10.1016/j.ijepes.2020.105877.

[15] W. Peres and N. N. da Costa, "Comparing strategies to damp electromechanical oscillations through STATCOM with multi-band controller," *ISA Trans.*, vol. 107, pp. 256–269, Dec. 2020, doi: 10.1016/j.isatra.2020.08.005.

[16] T. Surinkaew and I. Ngamroo, "Coordinated robust control of DFIG wind turbine and PSS for stabilization of power oscillations considering system uncertainties," *IEEE Trans. Sustain. Energy*, vol. 5, no. 3, pp. 823–833, Jul. 2014, doi: 10.1109/TSTE.2014.2308358.

[17] M. A. Hannan, N. N. Islam, A. Mohamed, M. S. H. Lipu, P. J. Ker, M. M. Rashid, and H. Shareef, "Artificial intelligent based damping controller optimization for the multi-machine power system: A review," *IEEE Access*, vol. 6, pp. 39574–39594, 2018, doi: 10.1109/ACCESS.2018.2855681.

[18] A. A. Alsakati, C. A. Vaithilingam, J. Alnasseir, and A. Jagadeeshwaran, "Investigation of single-band and multi-band power system stabilizers towards transient stability improvement in electrical networks," in *Proc. IEEE Conf. Energy Convers. (CENCON)*, Johor Bahru, Malaysia, Apr. 2021, pp. 196–201, doi: 10.1109/CENCON51869.2021.9627246.

[19] A. Khodabakhshian, R. Hemmati, and M. Moazzami, "Multi-band power system stabilizer design by using CPCE algorithm for multi-machine power system," *Electr. Power Syst. Res.*, vol. 101, pp. 36–48, Aug. 2013, doi: 10.1016/j.epsr.2013.03.011.

[20] *IEEE Recommended Practice for Excitation System Models for Power System Stability Studies*, IEEE Standard 421.5TM-2005 (Revision of IEEE Std 421.5-1992), Apr. 2006, pp. 1–93, doi: 10.1109/IEEESTD.2006.99499.

[21] I. Kamwa, R. Grondin, and G. Trudel, "IEEE PSS2B versus PSS4B: The limits of performance of modern power system stabilizers," *IEEE Trans. Power Syst.*, vol. 20, no. 2, pp. 903–915, May 2005, doi: 10.1109/TPWRS.2005.846197.

[22] Z. A. Obaid, M. T. Muhssin, and L. M. Cipcigan, "A model reference-based adaptive pss4b stabilizer for the multi-machines power system," *Electr. Eng.*, vol. 102, pp. 349–358, 2020, doi: 10.1007/s00202-019-00879-6.

[23] J. Huang, D. Rimorov, A. Moeini, I. Kamwa, A. Darvishi, B. Fardanesh, and S. Babaei, "Interconnection-level primary frequency control by MBPSS with wind generation and evaluation of economic impacts," *Int. J. Electr. Power Energy Syst.*, vol. 119, Jul. 2020, Art. no. 105867, doi: 10.1016/j.ijepes.2020.105867.

[24] C. Jauch, S. M. Islam, P. Sørensen, and B. B. Jensen, "Design of a wind turbine pitch angle controller for power system stabilisation," *Renew. Energy*, vol. 32, no. 14, pp. 2334–2349, Nov. 2007, doi: 10.1016/j.renene.2006.12.009.

[25] K. K. Sharma, A. Gupta, G. Kaur, R. Kumar, J. S. Chohan, S. Sharma, J. Singh, N. Khalilpoor, and A. Issakhov, "Power quality and transient analysis for a utility-tied interfaced distributed hybrid wind-hydro controls renewable energy generation system using generic and multiband power system stabilizers," *Energy Rep.*, vol. 7, pp. 5034–5044, Nov. 2021, doi: 10.1016/j.egyr.2021.08.031.

[26] Z. Li, T. Tiong, and K. Wong, "Transient stability improvement by using PSS4C in hybrid PV wind power system," in *Proc. 1st Int. Conf. Electr., Control Instrum. Eng. (ICECIE)*, Kuala Lumpur, Malaysia, 2019, pp. 1–6, doi: 10.1109/ICECIE47765.2019.8974751.

[27] D. Butti, S. K. Mangipudi, and S. R. Rayapudi, "An improved whale optimization algorithm for the design of multi-machine power system stabilizer," *Int. Trans. Electr. Energy Syst.*, vol. 30, no. 5, May 2020, doi: 10.1002/2050-7038.12314.

[28] A. Sabo, N. I. Abdul Wahab, M. L. Othman, M. Z. A. Mohd Jaffar, and H. Beiranvand, "Optimal design of power system stabilizer for multimachine power system using farmland fertility algorithm," *Int. Trans. Electr. Energy Syst.*, vol. 30, no. 12, Dec. 2020, Art. no. e12657, doi: 10.1002/2050-7038.12657.

[29] *IEEE Recommended Practice for Excitation System Models for Power System Stability Studies*, IEEE Standard 421.5TM-2016 (Revision of IEEE Std 421.5-2005), Aug. 2016, doi: 10.1109/IEEESTD.2016.7553421.

[30] P. M. Anderson and A. A. Fouad, *Power System Control and Stability*. Hoboken, NJ, USA: Wiley, 2003.

[31] A. A. Alsakati, C. A. Vaithilingam, K. Naidu, G. Rajendran, J. Alnasseir, and A. Jagadeeshwaran, "Particle swarm optimization for tuning power system stabilizer towards transient stability improvement in power system network," in *Proc. Int. Conf. Artif. Intell. Eng. Technol. (IICAIET)*, Kota Kinabalu, Malaysia, 2021, pp. 1–6, doi:, 10.1109/IICAIET51634.2021.9573534.

[32] A. A. Alsakati, C. A. Vaithilingam, J. Alnasseir, and A. Jagadeeshwaran, "Transient stability improvement of power system using power system stabilizer integrated with excitation system," in *Proc. 11th Int. Conf. Control Syst., Comput. Eng. (ICCSCE)*, Penang, Malaysia, 2021, pp. 34–39, doi: 10.1109/ICCSCE52189.2021.9530970.

[33] S. Mishra, M. Tripathy, and J. Nanda, "Multi-machine power system stabilizer design by rule based bacteria foraging," *Electr. Power Syst. Res.*, vol. 77, no. 12, pp. 1595–1607, 2007, doi: 10.1016/j.epsr.2006.11.006.

[34] P. Kundur, N. J. Balu, and M. G. Lauby, *Power System Stability and Control*. New York, NY, USA: McGraw- Hill, 1994.

[35] P. Rokni Nakhi and M. Ahmadi Kamarposhti, "Multi objective design of type II fuzzy based power system stabilizer for power system with wind farm turbine considering uncertainty," *Int. Trans. Electr. Energy Syst.*, vol. 30, no. 4, Apr. 2020, Art. no. e12285, doi: 10.1002/2050-7038.12285.

[36] M. Derafshian and N. Amjady, "Optimal design of power system stabilizer for power systems including doubly fed induction generator wind turbines," *Energy*, vol. 84, pp. 1–14, May 2015, doi: 10.1016/j.energy.2015.01.115.

[37] I. Kamwa. *(Hydro-Quebec) Performance of Three PSS for Interarea Oscillations—MATLAB & Simulink*. Accessed: Oct. 26, 2020. [Online]. Available: https://www.mathworks.com/help/physmod/sps/ug/performance-of-three-pss-for-interarea-oscillations.html

[38] C. V. Aravind, R. Rajparthiban, R. Rajprasad, I. Grace, R. Teymourzadeh, and M. Norhisam, "Mathematical toolbox and its application in the development of laboratory scale vertical axis wind turbine," in *Proc. Int. Conf. Power Energy (PECon)*, 2012, pp. 99–104, doi: 10.1109/PECon.2012.6450362.

[39] C. V. Aravind, R. Rajparthiban, R. Rajprasad, and Y. V. Wong, "A novel magnetic levitation assisted vertical axis wind turbine—Design procedure and analysis," in *Proc. 8th Int. Colloq. Signal Process. Appl.*, Malacca, Malaysia, 2012, pp. 93–98, doi: 10.1109/CSPA.2012.6194698.

[40] C. V. Aravind, S. Tay, A. Jagadeeswaran, and R. Firdaus, "Design analysis of MAGLEV-VAWT with modified magnetic circuit generator," in *Proc. 2nd Int. Conf. Electr. Energy Syst. (ICEES)*, Chennai, India, JJan. 2014, pp. 82–86, doi: 10.1109/ICEES.2014.6924146.

[41] M. S. A. Khan, K. R. Rajkumar, K. R. Rajkumar, and C. V. Aravind, "Optimization of multi-pole three phase permanent magnet synchronous generator for low speed vertical axis wind turbine," *Appl. Mech. Mater.*, vols. 446–447, pp. 704–708, Nov. 2014, doi: 10.4028/www.scientific.net/AMM.446-447.704.

[42] B. Ramlochun, C. A. Vaithilingam, A. A. Alsakati, and J. Alnasseir, "Transient stability analysis of IEEE 9-bus system integrated with DFIG and SCIG based wind turbines," *J. Phys., Conf. Ser.*, vol. 2120, no. 1, Dec. 2021, Art. no. 012023, doi: 10.1088/1742-6596/2120/1/012023.

[43] W. Peres, F. C. R. Coelho, and J. N. N. Costa, "A pole placement approach for multi-band power system stabilizer tuning," *Int. Trans. Electr. Energy Syst.*, vol. 30, no. 10, Oct. 2020, doi: 10.1002/2050-7038.12548.

[44] J. Kennedy and R. Eberhart, "Particle swarm optimization," in *Proc. Int. Conf. Neural Netw.*, Perth, WA, Australia, 1995, vol. 4, pp. 1942–1948, doi: 10.1109/ICNN.1995.488968.

[45] M. A. Abido, "Optimal design of power-system stabilizers using particle swarm optimization," *IEEE Trans. Energy Convers.*, vol. 17, no. 3, pp. 406–413, Sep. 2002, doi: 10.1109/TEC.2002.801992.

[46] W. Lin, Z. Lian, X. Gu, and B. Jiao, "A local and global search combined particle swarm optimization algorithm and its convergence analysis," *Math. Problems Eng.*, vol. 2014, pp. 1–11, Oct. 2014, doi: 10.1155/2014/905712.

[47] B. Dasu, M. Siva Kumar, and R. Srinivasa Rao, "Design of robust modified power system stabilizer for dynamic stability improvement using particle swarm optimization technique," *AIN Shams Eng. J.*, vol. 10, no. 4, pp. 769–783, Dec. 2019, doi: 10.1016/j.asej.2019.07.002.

[48] A. Oonsivilai and B. Marungsri, "Stability enhancement for multi-machine power system by optimal pid tuning of power system stabilizer using particle swarm optimization," *WSEAS Trans. Power Syst.*, vol. 3, no. 6, pp. 465–474, 2008.

AHMAD ADEL ALSAKATI (Graduate Student Member, IEEE) received the B.Eng. degree in electrical engineering and the master's degree in electrical power systems engineering from Damascus University, Syria, in 2007 and 2012, respectively. He is currently pursuing the Ph.D. degree with the School of Computer Science and Engineering, Taylor's University, Malaysia. His research interests include electrical power system operating, planning, and optimization. He also focuses on renewable energy integration power systems and the impact of distributed generation on power system stability.

CHOCKALINGAM ARAVIND VAITHILINGAM (Senior Member, IEEE) received the B.Eng. degree from Bharathiyar University, India, in 1998, the M.Eng. degree from Bharathidasan University, India, in 2001, and the Ph.D. degree in electrical power engineering from the Universiti Putra Malaysia, in 2013. He is currently heading the Electrical and Electronic Engineering Program, Faculty of Innovation and Technology, Taylor's University, Malaysia, and heading the Research Cluster VERTICALS aligned with SDG goals on sustainable energy and mobility (SDG 7, 11). He is a very frequent speaker at various international and national platforms. He is also a Professional Technologists with the Malaysian Board of Technologists. He is a member of IET, U.K. He is a member of the Society of Engineering Education Malaysia. He is a registered Chartered Engineer registered professional with the Engineering Council, U.K.

JAMAL ALNASSEIR received the B.Sc. degree in electrical engineering from Damascus University, Syria, in 1994, the Diploma degree in power system, in 1996, the master's degree in high voltage, in 2000, and the Ph.D. degree in electrical engineering from the University of Erlangen–Nuermberg, Germany, in 2007. He is currently an Associate Professor with the Electric Power Engineering Department, Damascus University. His research interests include high-voltage technology, power electronic, renewable energy sources, transient stability, and electrical networks.

KANENDRA NAIDU received the master's and Ph.D. degrees in electrical engineering from the University of Malaya, in 2011 and 2015, respectively. He is currently a Senior Lecturer with the Universiti Teknologi MARA (UiTM), Shah Alam. He is also a member of the Power System Planning and Operations Research Group (PoSPO). He also has strong working experience in a variety of evolutionary and swarm-based optimization techniques, graph theory, wavelet transform, and artificial neural networks. His research interest includes electrical engineering specializing in the implementation of artificial intelligence in power systems.

GOWTHAMRAJ RAJENDRAN (Graduate Student Member, IEEE) received the Bachelor of Engineering degree from the Government College of Engineering, Salem, India, in 2014, and the Master of Engineering degree (Hons.) from the PSG College of Technology, Coimbatore, India. He is currently pursuing the Ph.D. degree in electrical engineering with Taylor's University, Malaysia. He is working under the Research Cluster VERTICALS aligned with SDG goals on sustainable energy and mobility (SDG 7, 11). His current research is focused on the ac–dc power converters for electric vehicle charging stations. His research interest includes high-frequency semiconductor devices (silicon carbide and gallium nitride) for power converters in electric vehicle charging stations.